Room Temperature Terahertz Detection based on Plasma Resonance of Electrons in an Antenna-Coupled GaAs MESFET

Sangwoo Kim[a], Jeramy D. Zimmerman[b], Paolo Focardi[c], Dong Ho Wu[d], Arthur C. Gossard[b], and Mark S. Sherwin[a]
[a]Physics Department, University of California, Santa Barbara, CA 93106 USA
[b]Materials Department, University of California, Santa Barbara, CA 93106 USA
[C]Jet Propulsion Laboratory, Pasadena, CA 91109 USA
[d]Naval Research Laboratory, Washington D.C. 20375 USA

***Abstract*—Plasma resonance of electrons is observed in an Antenna-Coupled Metal-Semiconductor-Field-Effect-Transistor (MESFET) by sweeping bias voltages. This resonant absorption is exploited to realize a room temperature terahertz detector with a measured Noise Equivalent Power (NEP) ~ 5×10^{-8} W/Hz$^{1/2}$.**

I. Introduction And Background

TERAHERTZ (THz) detectors utilizing quantum transitions [1-4] require cryogenic temperatures since thermal energy (k_BT) needs to be smaller than the transition energy (1 THz ~ 4 meV ~ 50 K). A bulk (3-D) plasmon, corresponding to a collective excitation of an electron gas, is a classical excitation, and hence does not saturate with temperature. Plasma resonance occurs at a density-dependent frequency:

$$f_p = \frac{1}{2\pi}\sqrt{\frac{n_{3D}e^2}{m_e \varepsilon \varepsilon_0}}, \quad (1)$$

where n_{3D} is the 3-D free electron density, e is the charge of an electron, m_e is the effective mass of an electron, ε is the dielectric constant of the medium, and ε_0 is the permittivity of free space [5]. For 1 THz radiation, the corresponding 3-D free electron density is $n_{3D} \sim 10^{22}$ m^{-3} in GaAs, a density that can be easily achieved. Moreover, the density of the electrons can be made tunable if a device such as a Field-Effect-Transistor is employed. We utilize these facts in order to realize a room temperature THz detector. Our device consists of twin-slot antennas, coplanar waveguides, and a GaAs Metal-Semiconductor-Field-Effect-Transistor (MESFET) [3, 6]. The concept, fabrication, and performance of the first generation devices will be discussed.

II. Results

The measured figures of merit of the first set of devices, for example Noise Equivalent Power (NEP ~ 5×10^{-8} W/Hz$^{1/2}$) and electronics-limited response time (10 ns), are better than commercial pyroelectric detectors. Moreover, we were able to identify important device physics, including the plasma resonance of bulk electrons within the GaAs MESFET.

FIG. 1 shows a vertical cross-section of the GaAs MESFET, where dimensions of the gated active area are length 6 µm, width 3.3 µm, thickness 0.2 µm. The same gate voltage (V_G) was applied to the front and back gates. FIG. 2 shows detector responses to 4 µW, 1 THz radiation where V_G and drain voltage (V_D) were swept independently. There are two resonance features: One resonance occurs along the line V_D=-0.1 V. The other resonance is more prominent, and occurs along the line V_G-V_D=0.08 V. Moreover, the two peaks interfere destructively at their common resonance condition, V_G=-0.1 V and V_D=-0.18 V, the intersection of the dashed lines in FIG. 2.

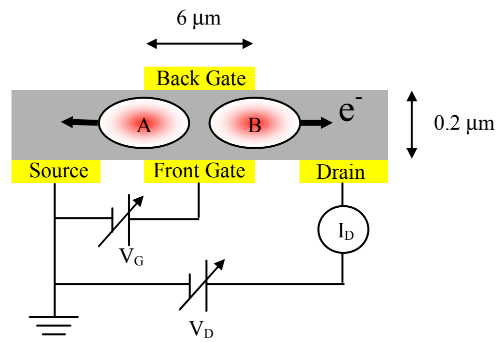

FIG. 1: Vertical cross-section of the GaAs MESFET. Electrons in the space-charge regions A and B are in resonance with incident THz radiation. Arrows indicate directions of photo-excited electrons

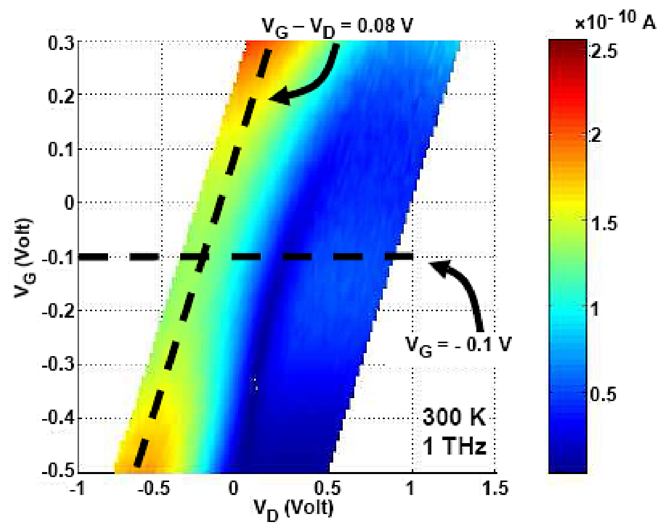

FIG. 2: Magnitude of detector responses to 1 THz radiation vs. V_D and V_G at 300K

These can be explained by considering two photovoltaic space-charge regions A and B in FIG. 1. Electrons in each region resonate with terahertz radiation under different bias conditions. For example, the density of electrons in region A increases monotonically with V_G, and hence goes through the

978-1-4244-2120-6/08/$25.00 ©IEEE.

plasma resonance at a certain V_G. In contrast, the density of electrons in region B increases with $V_G - V_D$, and hence goes through the plasma resonance at a certain $V_G - V_D$. Therefore the two resonance features in FIG. 2 can be associated with regions A and B in FIG. 1. In addition, the photovoltaic currents generated in the two regions are in opposite directions, causing some cancellation of the signal at the common resonance point.

Measurements were repeated at four different THz frequencies (0.14, 0.24, 0.6, 1 THz). For comparison, cross-sections of the data at $V_D = 0.5$ V are shown in FIG. 3(a). Each trace was rescaled and inserted with an appropriate vertical shift for clear presentation. In FIG. 3(a), resonance peaks associated with region A are visible. Also visible on the right hand side are the tails of resonance peaks associated with region B. The sharp turnarounds occur as the dominant contribution to the photocurrent changes from region A to region B and vice versa. Also observed upon the transition was a change of phase of the signal by 180 degree at the lock-in amplifier in R-θ mode, which supports the assumptions regarding the two photovoltaic space-charge regions. Data were fit to two Gaussian peaks and the peak positions were plotted vs. THz frequencies in FIG. 3(b), where the dependence of plasma resonance frequency to electron density (eq. (1)) is demonstrated. The dotted line is not a fit, but results from self-consistent simulations using a 1D-Poisson solver. An average electron density (n_{3D}) of the active region of the device was calculated with a gate voltage applied. The results at different gate voltages were used to generate the dotted line shown in FIG. 3(b) by matching gate voltages with corresponding resonance frequencies via eq. (1). FIG. 3(b) demonstrates that the resonance peaks shift as predicted by the plasma frequency - electron density relation (1). Benefits of our new concept and future outlook will be discussed.

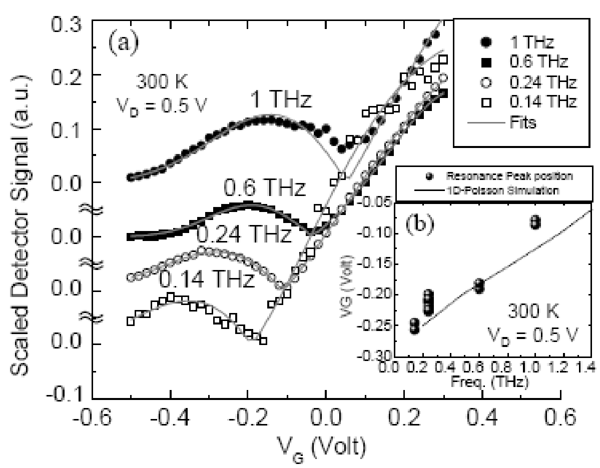

FIG. 3: (a) Cross-sections of the detector responses at $V_D = 0.5$ V for 0.14, 0.24, 0.6, 1 THz radiations. Sharp corners of the data are due to the change of the dominant contributor to the photocurrent between regions A and B. Solid curves are fits to the data. (b) Peak positions vs. THz frequencies. Dotted line was obtained from 1D-Poisson simulations.

Work supported by NSF-DMR 0703925 and Naval Research Lab.

References

[1] H. Schneider and H. C. Liu, *Quantum Well Infrared Photodetectors: Physics and Applications*, Springer Series in Optical Sciences Vol. 126, 2006

[2] C. L Cates *et al.*, Physica E **2**, 463-7 (1998)

[3] Mark S. Sherwin *et al.*, Proc. of 2002 Monterey submm workshop (http://www.sofia.usra.edu/det_workshop/papers/session6/6-03sherwin_edjw020913_2.pdf)

[4] G. B. Serapiglia et al., Proc. Of the Joint 30th Int. Conf. On IRMMW and THz Electronics, Sept. 19-23, 2005, IEEE Catalog Number 05EX1150C, p. 267

[5] J. D. Jackson, Classical Electrodynamics, 3rd edition, p.313 eq. (7.60)

[6] Paolo Focardi and Andrea Neto, IEEE Transactions on microwave theory and techniques, **53**, 1653 (2005)

978-1-4244-2120-6/08/$25.00 ©IEEE.